Binary homodyne detection for observing quadrature squeezing in satellite links

Christian R. Müller, Kaushik P. Seshadreesan, Christian Peuntinger, and Christoph Marquardt
Max Planck Institute for the Science of Light, Staudtstr. 2, 91058 Erlangen, Germany
and Institute of Optics, Information and Photonics, University of Erlangen-Nuremberg, Staudtstr. 7/B2, D-91058 Erlangen, Germany

(Received 14 June 2020; accepted 3 September 2020; published 30 September 2020)

Optical satellite links open up new prospects for realizing quantum physical experiments over unprecedented length scales. We analyze and affirm the feasibility of detecting quantum squeezing in an optical mode with homodyne detection of only one bit resolution, as is found in satellites already in orbit. We show experimentally that, in combination with a coherent displacement, a binary homodyne detector can still detect quantum squeezing efficiently even under high loss. The sample overhead in comparison to nondiscretized homodyne detection is merely a factor of 3.3.

DOI: 10.1103/PhysRevResearch.2.033523

I. INTRODUCTION

The laws of quantum mechanics have been validated by numerous fundamental tests [1]. With the advent of optical satellite links [2–6] it is now possible to also validate quantum mechanics over vast distances and varying gravitational potentials. The transmission and detection of nonclassical states [7] such as quadrature squeezed states of the light field [8,9] constitutes an important task in this regard. Squeezing is efficiently measured via homodyne detection [10], which is an important measurement technique not only in optics, but also in diverse physical architectures such as optomechanical resonators [11], superconducting qubits [12,13], spin ensembles [14–17], and Bose-Einstein condensates [18]. Homodyne detection yields continuously distributed quadrature projections, which in practice are sometimes deliberately discretized. In optical quantum information processing [19–23] this is exemplified by quantum key distribution (QKD) protocols [24] and by tests of Bell's inequalities [25–29], which inherently require one to discretize the homodyne outcomes to binary values.

Optical homodyne detectors are ubiquitous in telecommunications and can even be found on optical satellites already in orbit. Such satellites are thus promising candidates for exploring quantum technology and bringing fundamental tests of quantum mechanics to space both rapidly and cost-effectively. However, a very common use case of optical satellite links is classical communication via binary phase-shift keying. Since only the sign of the homodyne signal is relevant in this case, the measurement data in the detectors get deliberately projected into binary outcomes by signal processing [30,31]. The question then arises whether these detectors despite the strong technical constraint could be repurposed to detect, e.g., squeezed light. The challenge is compounded by the fact that satellite links can be tremendously lossy, which implies severely reduced observable squeezing values when quadrature-squeezed light is transmitted.

Extreme discretization into binary outcomes has been studied extensively for photon number measurements. Photon "on-off" detection and the photon number parity measurement were shown to allow for (near-) optimal applications in quantum state discrimination [32–36] and quantum optical metrology [37–42]. Discretized homodyne detection schemes were used for witnessing single-photon entanglement [43] and for super-resolved imaging with coherent states [44].

In this work, we investigate fundamental limits of discretized homodyne measurements, particularly focusing on the detection of quadrature squeezing. We consider the extreme case of a binary homodyne detector that simply distinguishes between positive and negative quadrature values, and we analyze its performance for the detection of individual signals as well as for the consecutive detection of multiple copies of the same state. We show that despite the extreme constraint, binary homodyne detection (BHD) can detect quadrature squeezing efficiently even under unfavorable conditions like high loss when relying on ensemble measurements. The ratio between the required number of copies to obtain the same information about the observed signal—measured in terms of the Bayesian *a posteriori* probability—is merely 3.3 and is independent of the squeezing parameter. We complement our theoretical analysis with an experimental verification. To this end, we prepare and detect both a coherent state and a weakly squeezed state via BHD and compare the results to ideal, i.e., nondiscretized, homodyne detection. We finally discuss the feasibility of detecting squeezed states via BHD in satellite links.

II. BINARY HOMODYNE DETECTION

In the following, we introduce the binary homodyne observable and describe how its expectation value can be controlled via a coherent displacement. We consider detecting

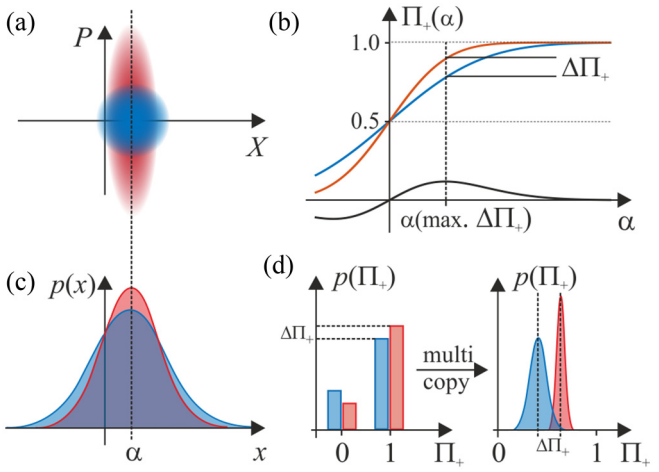

FIG. 1. (a) Illustration of a coherent (blue) and a displaced squeezed vacuum state (red) in phase space. (b) Binary homodyne expectation value Π_+ of the displaced states and their difference $\Delta\Pi_+(\alpha)$ (black) as a function of the displacement amplitude α. (c) Ideal homodyne marginal distributions along the squeezed x quadrature. (d) Sketch of the statistical BHD probability distribution $p(\Pi_+)$ obtained via single-copy and a multicopy detection.

a Gaussian state of a given quadrature uncertainty product, for which the ellipticity [23], i.e., the ratio between the major and minor semiaxis of its phase space distribution, has one of two possible values. The described detection scheme is agnostic to whether the Gaussian state is pure or mixed, i.e., whether the candidate states corresponding to the two values of ellipticity are squeezed vacuum states (states with quadrature uncertainty product equaling one unit of vacuum noise) or squeezed thermal states (states with quadrature uncertainty product in excess of one unit of vacuum noise). We will thus assume the former. Moreover, the overlap between any two states remains unchanged when applying the same squeezing operation to both. Therefore, we will assume that one of the candidate states is a coherent state (the most classical state as expected under the influence of high loss) and the other a squeezed state with the same mean amplitude as the coherent state, and with a real-valued squeezing parameter r [see Fig. 1(a)].

To identify the received signal via BHD, the signal is first displaced in phase space, followed by a projection onto quadrature semiaxes. This measurement is described by two positive operator-valued measure (POVM) elements:

$$\hat{\Pi}_+(\alpha) = \int_0^\infty dx\, \hat{D}^\dagger(\alpha)|x\rangle\langle x|\hat{D}(\alpha),$$
$$\hat{\Pi}_-(\alpha) = I - \hat{\Pi}_+(\alpha), \tag{1}$$

where α is the displacement amplitude. Owing to the symmetry along the quadrature axis, we can restrict the analysis to real and positive displacement amplitudes.

III. DECISION RULE

The BHD outcome is a Bernoulli random variable $Y(\alpha)$ over the sample space $y \in \{+, -\}$. The likelihood functions

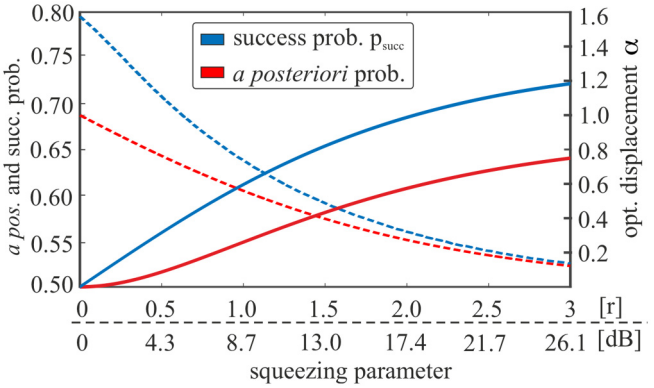

FIG. 2. Average *a posteriori* (red) and success probability (blue) for the detection of a single state, as well as the associated optimized displacement amplitudes α (dashed lines and right axis labels).

for the two hypotheses $\hat{\rho}_h \in \{\text{coh}, \text{sqz}\}$ are given by the conditional probabilities $P_{Y|H}(y|h) = \text{Tr}[\hat{\Pi}_y\, \hat{\rho}_h]$:

$$P_{Y|H}\left(\begin{smallmatrix}+\\-\end{smallmatrix}|\,\text{coh}, \alpha\right) = \frac{1}{2}\left[1 \pm \text{erf}\left(\frac{\alpha}{\sqrt{2}}\right)\right],$$
$$P_{Y|H}\left(\begin{smallmatrix}+\\-\end{smallmatrix}|\,\text{sqz}, \alpha, r\right) = \frac{1}{2}\left[1 \pm \text{erf}\left(\frac{\alpha}{\sqrt{2\,e^{-2r}}}\right)\right]. \tag{2}$$

The average *a posteriori* probability is derived by updating the priors ($P_H(\text{coh}) = P_H(\text{sqz}) = 1/2$) via Bayesian inference,

$$\langle P_{H|Y}(\alpha, r)\rangle = \sum_{y=\{+,-\}} \frac{\sum_h P_{Y|H}(y\,|\,h, \alpha, r)^2}{2\,P_Y(y)}, \tag{3}$$

where $P_Y(y) = (P_{Y|H}(y\,|\,\text{coh}) + P_{Y|H}(y\,|\,\text{sqz}))/2$, and is optimized over the displacement α.

For positive α, $P_{Y|H}(+|\,\text{sqz}) > P_{Y|H}(+|\,\text{coh})$, such that the squeezed state can be associated with the outcome "+" and the coherent state with the outcome "−." Figure 1(b) shows the BHD expectation value $\langle\Pi_+(\alpha)\rangle$. Varying the displacement amplitude allows maximizing the difference $\Delta\Pi_+ = P_{Y|H}(+\,|\,\text{sqz}) - P_{Y|H}(+\,|\,\text{coh})$ between the expectation values and consequently allows for an optimized discrimination. The maximal success probability for a single detection is

$$p_{\text{succ}} = \max_\alpha \frac{1 + \Pi_+(\alpha)}{2}. \tag{4}$$

The achievable success and *a posteriori* probability, as well as the associated optimized displacement amplitudes, are shown in Fig. 2 as a function of the squeezing parameter. Note that the displacement amplitudes optimizing the two parameters coincide only in the limit of large squeezing amplitudes. This emphasizes that *a posteriori* and success probability are indeed distinct figures of merit. The *a posteriori* probability is maximized by optimizing the difference between the conditional probabilities for any possible outcome, while the optimal success probability requires maximizing $\Delta\Pi_+$. The optimal displacement in the latter case coincides with the intersection point of the states' marginal distributions as

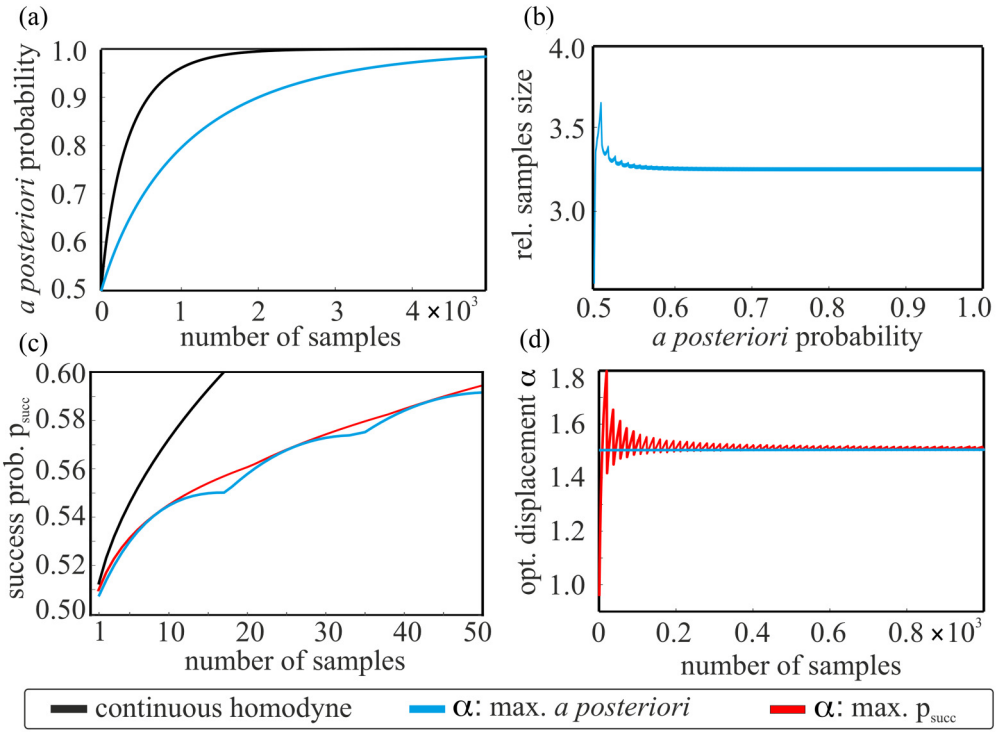

FIG. 3. (a) *A posteriori* probabilities for nondiscretized homodyne detection (black) and BHD as a function of the number of samples. The displacement is optimized for maximizing the *a posteriori* probability. (b) Relative sample overhead required to obtain the same *a posteriori* probability for the BHD measurement as obtained by nondiscretized homodyne detection. (c) Probability for successful state discrimination as a function of the number of samples and for different displacement strategies. (d) Comparison of the optimized displacement amplitudes α for different strategies.

depicted in Fig. 1(c):

$$\alpha^{(opt)}(r) = \sqrt{\frac{2r}{e^{2r}-1}}. \tag{5}$$

In the limit of an infinitely squeezed state the optimized displacement asymptotically approaches zero $\lim_{r\to\infty}\alpha(r) = 0$, but the success probability is upper bounded by $p_{\text{succ}} \leqslant \frac{3}{4}$, as at least half of the coherent state has support on the positive semiaxis. Similarly, the *a posteriori* probability is upper bounded by $\langle P_{H|Y}(\alpha, r)\rangle \leqslant \frac{2}{3}$.

IV. MULTICOPY DETECTION

To verify the properties of the quantum states after propagation it is sufficient to perform ensemble measurements. Gathering statistics over multiple measurements of identically prepared states allows reducing the overlap of the signals probability distributions [see Fig. 1(d)] and consequently reducing the error probability, defined as $1 - p_{\text{succ}}$. Let $\vec{y} = (y_1, y_2, \ldots, y_N)$ denote the outcome of a multicopy BHD measurement.

The probability to detect $k \in \{0, 1, \ldots, N\}$, positive quadrature projections from N measurements is given by the Binomial probability density function

$$P^{(N)}_{Y|H}(k|h,\alpha,r) = \binom{N}{k} P_{Y|H}(+|h,\alpha,r)^k \left[1 - P_{Y|H}(+|h,\alpha,r)\right]^{N-k}, \tag{6}$$

which approaches a quasicontinuous Gaussian distribution for a large number of samples.

The *a posteriori* probability for the signal hypothesis $h \in \{\text{coh}, \text{sqz}\}$ follows from the conditional single-copy probabilities in Eqs. (2) and (3) via Bayesian inference as

$$P^{(N)}_{H|\vec{Y}}(h|\vec{y}) = \frac{\prod_{i=1}^{N} P_{Y|H}(y_i|h)}{\sum_h \prod_{j=1}^{N} P_{Y|H}(y_j|h)}. \tag{7}$$

The maximal *a posteriori* probability is obtained by maximizing over the displacement parameter α and is given by

$$\left\langle P^{(N)}_{H|\vec{Y}} \right\rangle = \max_{\alpha} \sum_{k=0}^{N} \frac{\sum_h \left[P^{(N)}_{Y|H}(k\,|\,h,\alpha,r)\right]^2}{2\sum_{h'} P^{(N)}_{Y|H}(k\,|\,h',\alpha,r)}. \tag{8}$$

This quantity is compared to a nondiscretized homodyne detector in Fig. 3(a) for the example of a squeezing parameter $r = 0.085$, i.e., 0.369 dB below the shot-noise level. Naturally, the outcomes of the BHD yield less information about the detected states than ideal homodyne detection. (For details about the calculation of the *a posteriori* and success probability for ideal homodyne detection see Appendix A.) Consequently, a larger number of samples must be collected on average to achieve the same *a posteriori* probability. The required relative sample size is depicted in Fig. 3(b). Apart from the region of *a posteriori* probabilities close to 0.5, where statistical effects originating from the discreteness of the Binomial distribution are most pronounced, the ratio is essentially constant and has a value of merely 3.3. A separate

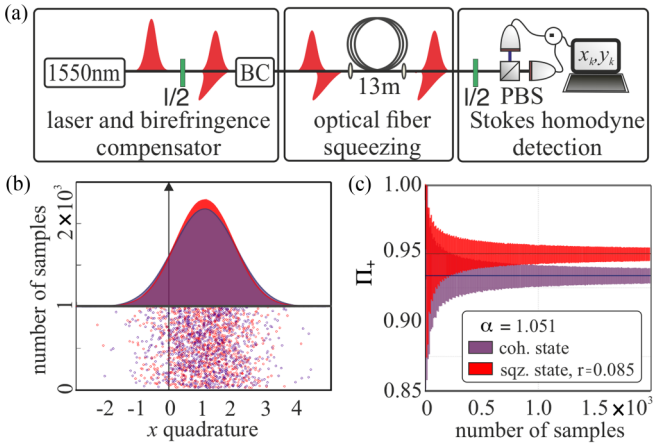

FIG. 4. (a) Outline of the experimental setup. (b) Measured marginal distributions of the coherent state (purple) and of the squeezed state (red) with $r = 0.085$, 0.369 dB. An excerpt of displaced homodyne samples for both states is displayed in the lower section. (c) Statistical distribution of the quadrature-parity observable as a function of the observed number of samples. The solid lines indicate the average quadrature parity.

analysis shows that this ratio is independent of the squeezing parameter r. We stress that this value, as it applies to the extreme discretization into binary outcomes, is indeed an upper bound for the required sample overhead of arbitrarily discretized homodyne detection such as occurring in realistic analog-to-digital (AD) converters.

The optimal success probability p_{succ} in multicopy detection is obtained by generalizing Eq. (4) such that the squeezed state is hypothesized whenever k equals or exceeds a threshold value τ, followed by maximizing over τ and α:

$$P^{(N)}_{\text{succ}}(k) = \max_{\alpha,\tau} \frac{P^{(N)}(k \leqslant \tau|\,\text{coh},\alpha) + P^{(N)}(k > \tau|\,\text{sqz},\alpha,r)}{2}. \tag{9}$$

Figure 3(c) compares the optimized success probability of BHD to that of ideal homodyne detection as well as to the success probability corresponding to BHD, where a displacement that maximizes the *a posteriori* probability is applied. Maximizing the *a posteriori* probability is equivalent to minimizing the error probability only in the limit of a large number of samples. This is underpinned in Fig. 3(d), where the distinct optimized displacements are illustrated. The fluctuations in the displacement maximizing the success probability originate from the discreteness of the underlying Binomial distribution. A more detailed discussion is given in Appendix B.

V. EXPERIMENTAL VALIDATION

We experimentally prepared a vacuum state and a weakly squeezed vacuum state ($r = 0.085$; 0.369 dB) using the fiber-based polarization squeezing setup [45] outlined in Fig. 4(a). Pulses from a shot-noise-limited laser centered at 1560 nm are distributed equally on the principal axes of a 13-m-long polarization maintaining fiber and get individually squeezed via the Kerr nonlinearity [46]. The emerging pulses are locked to circular polarization such that the mean value of the squeezed polarization state lies along the S_3 direction on the Poincaré sphere. Homodyne detection of the quantum Stokes variables within the *dark* S_1-S_2 plane is then equivalent to conventional homodyne detection in the canonical x-p phase space. A detailed description of the setup and the theoretical background can be found in Ref. [47]. In total, we acquired 2×10^8 homodyne samples $\{x_k\}$ of identically prepared copies of the vacuum and the squeezed state projected along the squeezed quadrature. The detector resolution is 16 bit, such that the quadrature was sampled quasicontinuously and the data provide accurate histograms of the actual marginal distribution as shown in Fig. 4(b). Applying a coherent displacement solely adds a *classical* offset amplitude to the quantum field operator, $\hat{a} \mapsto \hat{a} + \alpha$, and consequently to the detected quadrature, $\hat{X} \mapsto \hat{X} + \text{Re}(\alpha)$, where $\hat{X} = (\hat{a} + \hat{a}^\dagger)/2$. Therefore, given the quasicontinuous homodyne samples $\{x_k\}$, the coherent displacement and the subsequent projection onto the quadrature semiaxes $y_k \in \{+, -\}$ can faithfully be performed after detection via $x_k \mapsto y_k = \frac{1}{2}[\text{sgn}(x_k + \alpha) + 1]$.

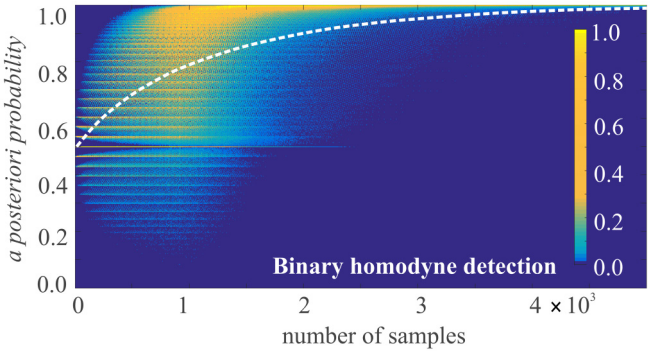

FIG. 5. Statistical distributions of the experimentally obtained *a posteriori* probabilities as a function of the number of detected samples N. For improved contrast, the maximal *a posteriori* probability for each value of N has been normalized to unity. The dashed white curve shows the average value for each number of detections.

The statistical distribution of the BHD samples for the measured coherent (purple) and squeezed state (red) are shown in Fig. 4(c) for a displacement amplitude $\alpha = 1.501$, which maximizes the *a posteriori* probability. The distributions are largely overlapping for a small number of samples but eventually become distinguishable with increasing sample size.

Figure 5 shows the experimentally obtained statistical distribution of the *a posteriori* probabilities for BHD as a function of the number of samples. The discreteness of the sample distributions yields a rich structure which is consistent with numerical simulations. For a large number of samples the *a posteriori* probability converges to unity as could be expected. The dashed white curve shows the average *a posteriori* probability, which also is in excellent agreement with theoretical predictions.

VI. OBSERVING SQUEEZING IN OPTICAL SATELLITE LINKS

Optical communication satellites are currently optimized for the detection of binary encoded classical signals. This encompasses projecting the signals into binary outcomes already

in the detection process, which thus prevents an evaluation of the continuous-variable (CV) quantum information. Our results on BHD pave the way to nevertheless detect quadrature squeezing in such scenarios. Let us investigate how the size of the measurement data required to faithfully detect a squeezed state scales as a function of loss in the transmission channel (see Appendix C for details). An up-link from a ground-based sender to a low Earth orbit (LEO) satellite receiver ($\approx$600 km distance) with transmitter and receiver apertures of about 30 cm diameter is subject to transmission losses of about 40–45 dB [48]. These losses includes atmospheric turbulence, diffraction, and pointing error. Let us further assume a moderate squeezing parameter of $r = 0.69$, corresponding to 6 dB of squeezing below the shot-noise level, and let us bound the average error probability to at most 10^{-2}. To satisfy this realistic scenario for 40 dB of loss, about 3×10^9 BHD samples are required, while 45 dB of loss would require 3×10^{10} samples. We stress again that this is of the same order of magnitude as the number of samples required by a nondiscretized homodyne detector, differing merely by a constant factor of 3.3. Optical homodyne detection and quadrature squeezing have been demonstrated with GHz bandwidths [49,50], such that the acquisition of the required number of samples can be achieved within a few seconds, i.e., well within the typical link time for a single flyover of a LEO satellite ($\approx$300 sec). We thus emphasize that it is, in principle, feasible with technology already in orbit to detect squeezing in optical satellite links.

Though our results establish that quantum squeezing can be detected using BHD even in the presence of high losses, it must be mentioned that useful quantum communication protocols involving squeezed states such as the protocols of Refs. [51,52] for CV QKD typically still require fine-grained homodyne detection to generate the raw keys. Moreover, it is well known that coherent states, which are much easier to prepare than squeezed states, are sufficient to perform CV QKD [53–55]. Coherent state protocols have been shown to be typically more tolerant to losses compared to squeezed state protocols (while the latter are interestingly more robust to excess noise than the former) [56,57]. Yet, even coherent state CV QKD protocols require fine-grained homodyne detection. Therefore, the existing optical satellite infrastructure is not equipped to support useful applications such as CV QKD. It is thus imperative to upgrade satellite equipment to enable high-rate CV quantum communications [58].

VII. CONCLUSIONS

Homodyne detection is a powerful quantum measurement even under the constraint of severe discretization. Our work underlines this by showing that a homodyne detector with a resolution of only one bit can still accomplish the quintessential task of detecting squeezed light efficiently. We derived the optimal phase space displacements for maximizing the success probability and the *a posteriori* probability, and found that a binary homodyne detector can distinguish two Gaussian states of different squeezing parameter with the same *a posteriori* probabilities as its nondiscretized counterpart by detecting a sample set merely a factor of 3.3 larger. Our work opens prospects for detecting quantum squeezing in optical satellite links. A possible early experimental demonstration might involve using (binary) homodyne detection on the satellite and an Earth-to-satellite communication link with a squeezer at the ground station that includes the necessary techniques for phase front precompensation and phase locking.

ACKNOWLEDGMENT

We thank Gerd Leuchs, Ulrik L. Andersen, and Dominique Elser for fruitful discussions.

APPENDIX A: *A POSTERIORI* PROBABILITIES FOR NONDISCRETIZED HOMODYNE DETECTION

The *a posteriori* probability for ideal, i.e., nondiscretized, homodyne detection is derived from the statistical distribution of the measured quadrature variance $\sigma_N^2 = \sum_{k=1}^{N} x_k^2/N$, where x_k are the continuous homodyne samples. The observed quadrature variance follows a χ_N^2 distribution, which is scaled such that the expectation value coincides with the mean quadrature variance of the detected state.

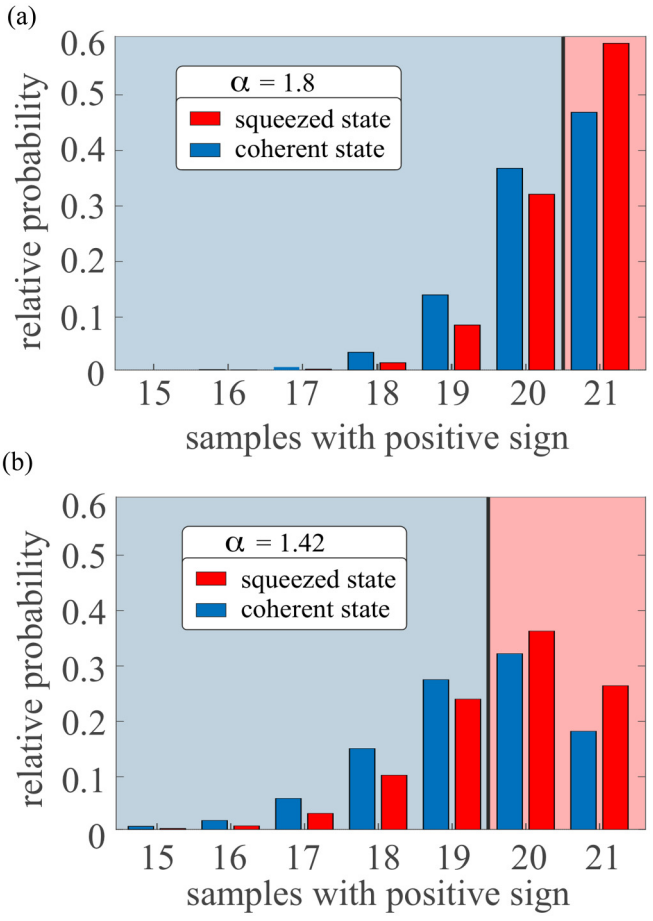

FIG. 6. Comparison of the statistical distributions for $N = 21$ samples and for different displacement amplitudes. (a) $\alpha = 1.8$: opt. displacement just before the discontinuity at $N = 20$. (b) $\alpha = 1.42$: opt. displacement just after the discontinuity at $N = 21$.

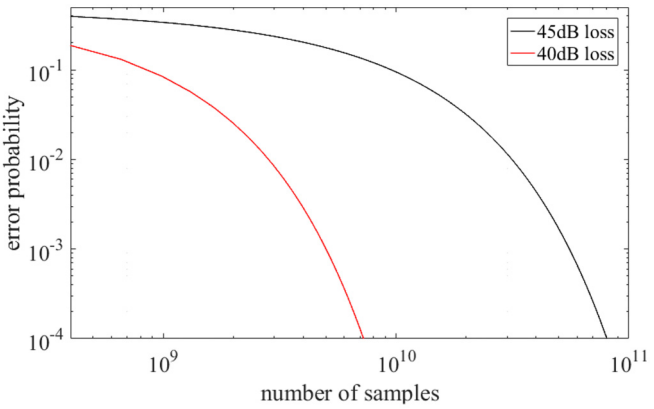

FIG. 7. Average minimum error probability as a function of the number of measured samples for the detection of a beam of light initially squeezed 6 dB below the shot-noise level at the output of a lossy channel of (a) 40 dB loss and (b) 45 dB loss.

Given the observation of the quadrature variance σ_N^2, the *a posteriori* probability for the hypothesis $h \in \{\text{coh}, \text{sqz}\}$ is

$$P_{H|Y}\left(h \,\middle|\, \sigma_N^2\right) = \frac{P_{Y|H}\left(\sigma_N^2 \middle| h\right)}{P_{Y|H}\left(\sigma_N^2 \middle| \text{coh}\right) + P_{Y|H}\left(\sigma_N^2 \middle| \text{sqz}\right)}. \quad \text{(A1)}$$

The average *a posteriori* probability is obtained via integration over the scaled χ_N^2 probability distribution for observing the quadrature variance σ_N^2:

$$\langle P_H \rangle = \frac{1}{2} \sum_h \int_0^\infty P_{Y|H}\left(\sigma_N^2 \middle| h\right) \cdot P_{H|Y}\left(h \,\middle|\, \sigma_N^2\right) d\sigma_N^2. \quad \text{(A2)}$$

In the state discrimination scenario, the state with the higher *a posteriori* probability $\langle P_H(h) \rangle$ is hypothesized:

$$P_{H|Y}\left(\text{sqz}\middle|\sigma_N^2\right) \underset{H=\text{coh}}{\overset{H=\text{sqz}}{>}} P_{H|Y}\left(\text{coh}\middle|\sigma_N^2\right). \quad \text{(A3)}$$

APPENDIX B: DISCONTINUOUS OPTIMAL DISPLACEMENT AMPLITUDE IN MAXIMIZING THE SUCCESS PROBABILITY

The Binomial probability density functions [see Eq. (6)] for the projection of 21 copies of the coherent state and the squeezed state onto the positive quadrature semiaxis Π_+ are shown for different displacement amplitudes α in Fig. 6. The blue-shaded areas indicates the cumulative quadrature projections that lead to the hypothesis for the coherent state, while outcomes in the red-shaded area are identified as the squeezed state. The distribution in Fig. 6(a) is obtained with the displacement amplitude maximizing the success probability for $N = 20$ copies, $\alpha = 1.8$, i.e., just before the discontinuity. In this configuration, the measurement hypothesizes the squeezed state only if all ($k = 21$) detected states are projected onto a positive quadrature value. Figure 6(b) shows the distribution at the actual optimal displacement amplitude $\alpha = 1.42$. The state is identified as the squeezed state if $k = 20$ or $k = 21$ detections had a positive quadrature projection. The discontinuities in the optimized displacement curve result from discrete shifts in the decision threshold combined with the maximization of the likelihoods of the coherent and squeezed state distributions on their respective identification domains. For a large number of copies N the range of possible outcomes approaches a quasicontinuous Gaussian distribution, and the optimized displacement approaches an asymptotically optimal value.

APPENDIX C: REQUIRED SAMPLES SIZE FOR SQUEEZING DETECTION IN LEO SATELLITE LINKS

Figure 7 depicts the error probability for the unbiased detection of squeezed states (6 dB, $r = 0.69$) emerging from a lossy channel of 40 dB and 45 dB, respectively [59]. On an absolute scale, the error probability remains nearly constant up to a certain number of detected samples, but thereafter drops steeply with increasing number of samples. The plot shows that squeezing can be detected with an average error probability no greater than 10^{-2} by measuring 3×10^9 (40 dB) samples and 3×10^{10} (45 dB) samples, respectively.

[1] P. Shadbolt, J. C. F. Mathews, A. Laing, and J. L. O'Brien, Nat. Phys. **10**, 278 (2014).

[2] J. G. Rarity, P. R. Tapster, P. M. Gorman, and P. Knight, New J. Phys. **4**, 82 (2002).

[3] R. Ursin, T. Jennewein, J. Kofler, J. M. Perdigues, L. Cacciapuoti, C. J. de Matos, M. Aspelmeyer, A. Valencia, T. Scheidl, A. Acin *et al.*, Europhys. News **40**, 26 (2009).

[4] Z. Merali, Nature (London) **492**, 22 (2012).

[5] K. Günthner, I. Khan, D. Elser, B. Stiller, O. Bayraktar, C. R. Müller, K. Sauke, D. Tröndle, F. Heine, S. Seel *et al.*, Optica **4**, 611 (2017).

[6] F. Vedovato, C. Agnesi, M. Schiavon, D. Dequal, L. Calderaro, M. Tomasin, D. Giacomo Marangon, A. Stanco, V. Luceri *et al.*, Sci. Adv. **3**, e1701180 (2017).

[7] D. Rideout, T. Jennewein, G. Amelino-Camelia, T. F. Demarie, B. L. Higgins, A. Kempf, A. Kent, R. Laflamme, X. Ma, R. B. Mann *et al.*, Classical Quantum Gravity **29**, 224011 (2012).

[8] C. Weedbrook, S. Pirandola, R. García-Patrón, N. J. Cerf, T. C. Ralph, J. H. Shapiro, and S. Lloyd, Rev. Mod. Phys. **84**, 621 (2012).

[9] U. L. Andersen, T. Gehring, C. Marquardt, and G. Leuchs, Phys. Scr. **91**, 053001 (2016).

[10] H. P. Yuen and V. W. S. Chan, Opt. Lett. **8**, 177 (1983).

[11] M. Aspelmeyer, T. J. Kippenberg, and F. Marquardt, Rev. Mod. Phys. **86**, 1391 (2014).

[12] A. A. Houck, D. I. Schuster, J. M. Gambetta, J. A. Schreier, B. R. Johnson, J. M. Chow, L. Frunzio, J. Majer, M. H. Devoret, S. M. Girvin, and R. J. Schoelkopf, Nature **449**, 328 (2007).

[13] S. Filipp, P. Maurer, P. J. Leek, M. Baur, R. Bianchetti, J. M. Fink, M. Göppl, L. Steffen, J. M. Gambetta, A. Blais, and A. Wallraff, Phys. Rev. Lett. **102**, 200402 (2009).

[14] A. Kuzmich and E. S. Polzik, in *Quantum Information with Continuous Variables*, edited by S. L. Braunstein and A. K. Pati, (Springer, Dordrecht, 2003), pp. 231–265.

[15] N. J. Cerf, G. Leuchs, and E. S. Polzik, *Quantum Information with Continuous Variables of Atoms and Light* (Imperial College Press, London, 2007).

[16] R. Namiki, S. I. R. Tanaka, T. Takano, and Y. Takahashi, Appl. Phys. B **105**, 197 (2011).

[17] C. R. Müller, L. S. Madsen, A. B. Klimov, L. L. Sánchez-Soto, G. Leuchs, C. Marquardt, and U. L. Andersen, Phys. Rev. A **93**, 033816 (2016).

[18] J. Estéve, C. Gross, A. Weller, S. Giovanazzi, and M. K. Oberthaler, Nature (London) **455**, 1216 (2008).

[19] S. L. Braunstein and P. van Loock, Rev. Mod. Phys. **77**, 513 (2005).

[20] D. T. Smithey, M. Beck, M. G. Raymer, and A. Faridani, Phys. Rev. Lett. **70**, 1244 (1993).

[21] U. Leonhardt, *Measuring the Quantum State of Light* (Cambridge University Press, Cambridge, 1997).

[22] A. I. Lvovsky and M. G. Raymer, Rev. Mod. Phys. **81**, 299 (2009).

[23] C. R. Müller, C. Peuntinger, T. Dirmeier, I. Khan, U. Vogl, C. Marquardt, G. Leuchs, L. L. Sánchez-Soto, Y. S. Teo, Z. Hradil, and J. Řeháček, Phys. Rev. Lett. **117**, 070801 (2016).

[24] Y.-B. Zhao, M. Heid, J. Rigas, and N. Lütkenhaus, Phys. Rev. A **79**, 012307 (2009).

[25] A. Gilchrist, P. Deuar, and M. D. Reid, Phys. Rev. A **60**, 4259 (1999).

[26] W. J. Munro, Phys. Rev. A **59**, 4197 (1999).

[27] G. Auberson, G. Mahoux, S. Roy, and V. Singh, Phys. Lett. A **300**, 327 (2002).

[28] K. Banaszek and K. Wódkiewicz, Phys. Rev. Lett. **82**, 2009 (1999).

[29] K. P. Seshadreesan, C. F. Wildfeuer, M. B. Kim, H. Lee, and J. P. Dowling, Quantum Inf. Process. **15**, 1025 (2016).

[30] S. Schaefer, M. Gregory, and W. Rosenkranz, Opt. Eng. **55**, 111614 (2016).

[31] F. Heine, G. Mühlnikel, H. Zech, D. Tröndle, S. Seel, M. Motzigemba, R. Meyer, S. Philipp-May, and E. Benzi, Proc. SPIE **9354**, 133 (2015).

[32] S. J. Dolinar, An optimum receiver for the binary coherent state quantum channel, Quarterly Progress Report 111, MIT Research Laboratory of Electronics, Cambridge, MA, 1973, pp. 115–120.

[33] C. Wittmann, M. Takeoka, K. N. Cassemiro, M. Sasaki, G. Leuchs, and U. L. Andersen, Phys. Rev. Lett. **101**, 210501 (2008).

[34] M. Takeoka and M. Sasaki, Phys. Rev. A **78**, 022320 (2008).

[35] C. Wittmann, U. L. Andersen, M. Takeoka, D. Sych, and G. Leuchs, Phys. Rev. Lett. **104**, 100505 (2010).

[36] M. M. Wilde, S. Guha, S. H. Tan, and S. Lloyd, in *Proceedings of the 2012 IEEE International Symposium on Information Theory (ISIT)* (IEEE, Piscataway, 2012), pp. 551–555.

[37] J. P. Dowling and K. P. Seshadreesan, J. Lightwave Technol. **33**, 2359 (2015).

[38] R. Demkowicz-Dobrzański, M. Jarzyna, and J. Kołodyński, Prog. Opt. **60**, 345 (2015).

[39] K. P. Seshadreesan, S. Kim, J. P. Dowling, and H. Lee, Phys. Rev. A **87**, 043833 (2013).

[40] K. P. Seshadreesan, P. M. Anisimov, H. Lee, and J. P. Dowling, New J. Phys. **13**, 083026 (2011).

[41] P. M. Anisimov, G. M. Raterman, A. Chiruvelli, W. N. Plick, S. D. Huver, H. Lee, and J. P. Dowling, Phys. Rev. Lett. **104**, 103602 (2010).

[42] K. R. Motes, J. P. Olson, E. J. Rabeaux, J. P. Dowling, S. J. Olson, and P. P. Rohde, Phys. Rev. Lett. **114**, 170802 (2015).

[43] O. Morin, J.-D. Bancal, M. Ho, P. Sekatski, V. D'Auria, N. Gisin, J. Laurat, and N. Sangouard, Phys. Rev. Lett. **110**, 130401 (2013).

[44] E. Distante, M. Ježek, and U. L. Andersen, Phys. Rev. Lett. **111**, 033603 (2013).

[45] J. Heersink, V. Josse, G. Leuchs, and U. L. Andersen, Opt. Lett. **30**, 1192 (2005).

[46] M. Kitagawa and Y. Yamamoto, Phys. Rev. A **34**, 3974 (1986).

[47] C. R. Müller, B. Stoklasa, C. Peuntinger, C. Gabriel, J. Řeháček, Z. Hradil, A. B. Klimov, G. Leuchs, C. Marquardt, and L. L. Sánchez-Soto, New J. Phys. **14**, 085002 (2012).

[48] J.-P. Bourgoin, E. Meyer-Scott, B. L. Higgins, B. Helou, C. Erven, H. Hübel, B. Kumar, D. Hudson, I. D'Souza, R. Girard *et al.*, New J. Phys. **15**, 023006 (2013).

[49] C. Gabriel, C. Wittmann, B. Hacker, W. Mauerer, E. Huntington, M. Sabuncu, C. Marquardt, and G. Leuchs, in *Conference on Lasers and Electro-Optics 2012* (Optical Society of America, 2012), p. JW4A.103.

[50] S. Ast, M. Mehmet, and R. Schnabel, Opt. Express **21**, 13572 (2013).

[51] N. J. Cerf, M. Lévy, and G. Van Assche, Phys. Rev. A **63**, 052311 (2001).

[52] R. García-Patrón and N. J. Cerf, Phys. Rev. Lett. **102**, 130501 (2009).

[53] F. Grosshans, G. Van Assche, J. Wenger, R. Brouri, N. J. Cerf, and P. Grangier, Nature (London) **421**, 238 (2003).

[54] C. Weedbrook, A. M. Lance, W. P. Bowen, T. Symul, T. C. Ralph, and P. K. Lam, Phys. Rev. Lett. **93**, 170504 (2004).

[55] J. Lin, T. Upadhyaya, and N. Lütkenhaus, Phys. Rev. X **9**, 041064 (2019).

[56] M. Navascués and A. Acín, Phys. Rev. Lett. **94**, 020505 (2005).

[57] R. García-Patrón and N. J. Cerf, Phys. Rev. Lett. **97**, 190503 (2006).

[58] N. Hosseinidehaj, Z. Babar, R. Malaney, S. X. Ng, and L. Hanzo, IEEE Commun. Surv. Tutorials **21**, 881 (2019).

[59] C. R. Müller, K. P. Seshadreesan, G. Leuchs, and C. Marquardt, in *Proceedings of the 2017 IEEE International Conference on Space Optical Systems and Applications (ICSOS)* (IEEE, Piscataway, 2017), pp. 307–311.